

Probing the near-horizon region of Cygnus X-1 with *Suzaku* and *NuSTAR*

Zuobin Zhang,¹ Honghui Liu,¹ Askar B. Abdikamalov,^{1,2} Dmitry Ayzenberg,³ Cosimo Bambi,^{1,*} and Menglei Zhou⁴

¹*Center for Field Theory and Particle Physics and Department of Physics, Fudan University, 200438 Shanghai, China*

²*Ulugh Beg Astronomical Institute, Tashkent 100052, Uzbekistan*

³*Theoretical Astrophysics, Eberhard-Karls Universität Tübingen, D-72076 Tübingen, Germany*

⁴*Institut für Astronomie und Astrophysik, Eberhard-Karls Universität Tübingen, D-72076 Tübingen, Germany*

Astrophysical black holes are ideal laboratories for testing Einstein’s theory of general relativity in the strong field regime. In this manuscript, we present an analysis of *Suzaku* and *NuSTAR* spectra of the black hole binary Cygnus X-1 using `relxill_nk`. Unlike our previous study on Cygnus X-1 with *NuSTAR* data, here we are able to constrain the Johannsen deformation parameter α_{13} . However, despite the high energy resolution near the iron line provided by *Suzaku*, our constraints on the Kerr metric from Cygnus X-1 are not very stringent in comparison with those that have been obtained from other sources, confirming that Cygnus X-1 is quite a complicated source.

I. INTRODUCTION

Einstein’s theory of general relativity was proposed over a century ago and so far has successfully passed a large number of observational tests. Since the 1960s, there have been significant efforts to test general relativity in the so-called weak field regime with experiments in the Solar System and observations of binary pulsars [1]. In the past 20 years, there has been an increasing interest in testing general relativity on large scales with cosmological tests, which are mainly motivated by the problems of dark matter and dark energy [2–4]. Thanks to new observational facilities, the past 5 years have seen a tremendous progress on tests of general relativity in the so-called strong field regime, and we are now starting testing the predictions of Einstein’s gravity in the strong gravitational field of black holes [5–16].

The spacetime metric around astrophysical black holes is thought to be approximated well by the Kerr solution [17], since the possible electric charge of the object or the gravitational field produced by the accretion disk or nearby stars is normally completely negligible in the near-horizon region [18–20]. However, a number of authors have pointed out that new physics may produce macroscopic deviations from the Kerr solution, because general relativity may not be the correct theory of gravity, there may be large quantum gravity effects, or because of the presence of exotic matter fields; see, e.g. Refs. [21–25].

As of now, tests of general relativity in the strong gravity regime using black holes are possible by studying the gravitational wave signal from the coalescence of stellar-mass black holes (e.g. [5, 6, 15, 16]), by studying the properties of the X-ray radiation emitted from the inner part of the accretion disk (e.g. [8, 9, 11, 12, 14]), or by studying the image of the supermassive black holes in the galaxy M87 (e.g. [10, 13]). In the past few years, our group has mainly worked on X-ray tests by developing the relativistic reflection model `relxill_nk` [26, 27],

which is an extension of the `relxill` package [28–30] to non-Kerr spacetimes. In addition to the parameters present in `relxill`, `relxill_nk` has some “deformation parameters” to quantify possible deviations from the Kerr geometry, which is recovered when all deformation parameters vanish. The reflection spectrum of the accretion disk is calculated without assuming that these deformation parameters vanish. From the comparison of the theoretical model with the observational data, it is possible to estimate the value of the deformation parameters and check whether the observations are consistent with the hypothesis that the spacetime metric around astrophysical black holes is described by the Kerr solution as expected in the standard framework. Like most astrophysical measurements, the accuracy of the estimate of the deformation parameters depends on the capability of the theoretical model to properly describe the astrophysical system and it is thus very important to select the sources and the observations that are expected to match better the characteristics of the theoretical model in order to limit undesirable systematic uncertainties.

The origin of the reflection spectrum of the disk can be understood as follows. We consider a black hole accreting from a geometrically thin and optically thick disk. The thermal spectrum of the disk is peaked in the soft X-ray band in the case of stellar-mass black holes and in the optical/UV band in the case of supermassive black holes. Thermal photons from the disk inverse Compton scatter off free electrons in the corona, which is some hotter (~ 100 keV) cloud near the black hole and the inner part of the accretion disk, even if its morphology is not yet well understood. The Comptonized photons have a power-law spectrum with a high-energy cut-off and can illuminate the accretion disk, producing a reflection component. The latter is characterized by some fluorescent emission lines below 10 keV, notably the iron $K\alpha$ complex, and by a Compton hump peaked at 20–30 keV. The analysis of the reflection features can be used to study the morphology of the accreting matter, measure black hole spins, and test Einstein’s theory of general relativity in the strong field regime [31, 32].

The analysis of relativistic reflection features requires

* Corresponding author: bambi@fudan.edu.cn

both a good energy resolution near the iron line and data over a broad energy band. The good energy resolution near the iron line is useful because the shape of the iron $K\alpha$ line is the most informative part of the spectrum concerning the motion of the gas in the very strong gravity region around the black hole. The broad energy band helps to select the correct astrophysical model and to constrain better some disk-related parameters that, in turn, help to measure better the parameters of the spacetime metric.

In Ref. [33], we analyzed with `relxill_nk` two *NuSTAR* observations of Cygnus X-1, respectively in 2012 and 2014, when the source was in the soft state. We found it very challenging to test the Kerr metric from those spectra, in the sense that our measurements of the deformation parameters could easily change by changing some assumptions like the emissivity profile model for the accretion disk. Similar problems were met with the analysis of a *NuSTAR* observation of GRS 1915+105 [34] and of *RXTE* data of GX 339-4 [35]. On the contrary, very promising results have been found from the analysis of *Suzaku* and *XMM-Newton*+*NuSTAR* observations of other sources [9, 36, 37], suggesting the possibility that for testing the Kerr metric it is strictly necessary to have a good energy resolution near the iron line. In the present paper, we thus analyze a 2009 *Suzaku* observation of Cygnus X-1 in the hard state and a simultaneous observation *Suzaku*+*NuSTAR* in 2012 when Cygnus X-1 was in the soft state.

Our manuscript is organized as follows. In Section II, we present the *Suzaku* and *NuSTAR* observations analyzed in our work and we describe their data reduction. In Section III, we report the analysis of the 2009 *Suzaku* observation, when the source was in the hard state. Section IV is devoted to the analysis of the simultaneous observations *Suzaku*+*NuSTAR* in 2012, when Cygnus X-1 was in the soft state. We discuss our results in Section V.

II. OBSERVATIONS AND DATA REDUCTION

Cygnus X-1 was discovered in 1964 during a rocket flight and is one of the brightest X-ray sources in the sky. It is a binary system with a black hole with a mass of $14.8 \pm 1.0 M_{\odot}$ [38] and a type O9.7Iab supergiant companion star. The strong wind from the companion star provides a sufficiently high mass transfer to the black hole at any time, so Cygnus X-1 is a persistent X-ray source. The distance of this binary system from us is $1.86^{+0.12}_{-0.11}$ kpc [39].

In the present work, we consider the *Suzaku* [40] and *NuSTAR* [41] observations listed in Tab. I. The first observation (epoch 1) was in 2009 by *Suzaku*, when the source was in a hard state. The second observation (epoch 2) refers to a simultaneous observation of *Suzaku* and *NuSTAR* in 2012, when the source was in a soft state. Spectra from the data are created by using the tools from the HEASOFT 6.26 package: version

20181023 of *Suzaku* Calibration Database (CALDB) for the *Suzaku* data and version 20180419 of *NuSTAR* Calibration Database (CALDB) for the *NuSTAR* data.

A. *Suzaku* data in the hard state

The *Suzaku* satellite was equipped with three detectors (XISs, HXD/PIN, and HXD/GSO), through which *Suzaku* could cover the 0.3-600 keV band. During the observation of the epoch 1, only XIS0, XIS3, PIN, and GSO detectors were operational. The XIS data are reduced following the standard procedure, which includes `xispi` for energy scale reprocessing and `xisrepro` for data screening. For each event file, we use the `aeattcor2` tool to correct the data for large spacecraft wobble endemic to *Suzaku*.

An issue in the *Suzaku* data of Cygnus X-1 is the presence of photon pile-up, as a consequence of the brightness of the source. To minimize the pile-up effect, we use the FTOOL `pileest` to estimate the pile-up degree and thus exclude the most heavily piled-up region. Finally, we extract the spectra from a square box, 240 pixels on each side, with an inner exclusion circle with a radius of 30 pixels, which is centered on the source coordinates. This effectively reduced the pile-up on the extracted region to 5% or less. The redistribution matrix files and ancillary response files are constructed by the tool `xisrmfgen` and `xissimarfgen`, respectively. Since the XIS0 and XIS3 CCDs are both front-illuminated chips and have similar response function, we use `addascaspec` to combine their spectra, backgrounds, and response functions. We then grouped the spectra to have at least 10 counts per bin as done in [42].

The HXD/PIN and HXD/GSO spectra are generated and reduced using the FTOOL `hxdpinxbpi` and `hxdgsoxbpi`, respectively. The corresponding background and response (including the “correction arf”) files are downloaded from the `pinxb_ver2.0_tuned` and `gsonxb_ver2.0` directory at HEASARC. Eventually, we analyze the data in the 0.8-1.7 keV and 2.5-9.0 keV bands for the XIS spectra, the 12-70 keV band for PIN, and 70-500 keV band for GSO.

B. *Suzaku* data in the soft state

For the *Suzaku* observation 407072010, we proceed in a similar way. Since the source was in the soft state, the data are more heavily affected by pile-up than those of the 2009 observation. The spectra are extracted from a rectangular region, approximately 320×220 pixels, with two inner exclusion rectangles with the size of 130×45 pixels, centered on the source coordinates. This effectively reduced the pile-up on the extracted region to 5% or less. Because the XIS0 CCD has front-illuminated chips while XIS1 has back-illuminated chips, the spectra were separately grouped using the tool `grppha` so that

Epoch	State	Mission	Obs. ID	Instrument(s)	Start date	Exposure (ks)	
1	Hard	<i>Suzaku</i>	404075020	XIS0+3	2009-04-08	10.7	
				HXD/PIN		12.2	
				HXD/GSO		12.2	
2	Soft	<i>Suzaku</i>	407072010	XIS0+1	2012-10-31	1.9	
				HXD/PIN		30.1	
				HXD/GSO		27.9	
		<i>NuSTAR</i>	30001011002	30001011003	FPMA+FPMB	2012-10-31	11.0
					FPMA+FPMB		5.7
		10014001001	FPMA+FPMB		4.6		

TABLE I. Summary of the observations analyzed in the present work.

each bin have at least 50 counts. For the HXD/PIN and HXD/GSO data, we still used, respectively, the FTOOL `hxdpinxbpi` and `hxdgsoxbpi` to extract the spectra. We use data in the 1.2-1.7 keV and 2.5-9.0 keV band from XIS, 15-68 keV band from PIN, and 50-296 keV band from GSO.

C. *NuSTAR* data in the soft state

We reduce the data from instruments Focal Plane Modules A and B (FPMA and FPMB). We separately reduce the data of the three observations and then use `addascaspec` to combine the spectra for each FPM instrument. We run `nuproduct` to extract light curves, spectra, and response files. The source is extracted from a circular region centered on Cygnus X-1 with a radius of $150''$. The background region is a circle with the same size taken far from the source region to avoid any contribution from the source. The spectra are then grouped to have a minimum count of 50 photons per bin.

III. ANALYSIS OF EPOCH 1

Here and in the next section, we use XSPEC v12.10.1s for the spectral analysis [43]. The Galactic absorption is fitted with `tbabs` [44]. The relativistic reflection component is fitted with `relxill_nk` v1.3.3 [26, 27]. The spacetime metric around the black hole is described by the Johannsen metric with the deformation parameter α_{13} , while all other deformation parameters vanish [45].

To start, we fit the 2009 *Suzaku* data with a simple power law. The resulting spectrum and data-to-model ratio are shown in Fig. 1. We clearly see an excess of photons below 2 keV, a small feature around 6-7 keV, and a bump in the HXD data. The excess of photons at low energies suggests the presence of the thermal component from the accretion disk. The small feature at 6-7 keV and the bump can be naturally interpreted as an iron line and a Compton hump from the reflection spectrum.

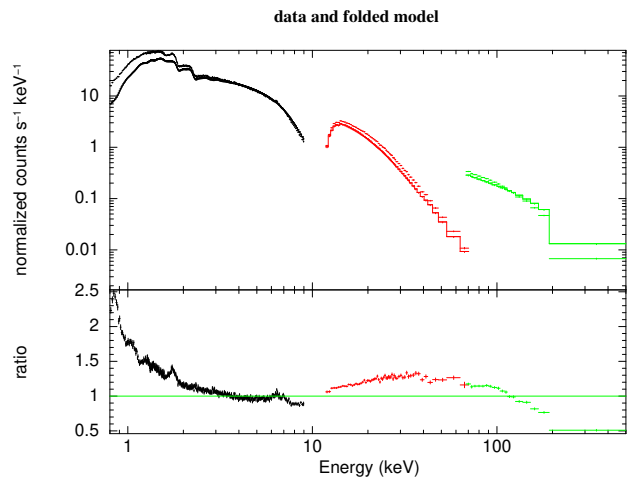


FIG. 1. The upper quadrant shows the spectrum of Cygnus X-1 in epoch 1 as seen by XIS0+XIS3 (black), PIN (red) and GSO (green). The spectrum is fitted with an absorbed power-law ignoring the data below 3 keV, the 5-7 keV band, and the 15-45 keV band. The data to the best-fit model ratio is shown in the lower quadrant. The data have been rebinned for visual clarity.

The models used to fit the 2009 *Suzaku* data are summarized in Tab. II. We use `diskbb` to describe the thermal spectrum of the accretion disk [46]. We use `relxill_nk` to fit the reflection spectrum setting the reflection fraction to -1 and using `cutoffpl` to describe the Comptonized photons from the corona. We find that we can get a better fit adding a Gaussian emission line. Eventually the XSPEC model is (Model 1):

`tbabs×xstar×(diskbb+cutoffpl+gauss+relxill_nk)`, where `xstar` describes an ionized plasma in the wind from the companion star. A multiplicative constant is added to combine the data from different instruments. In `relxill_nk`, we use a broken power-law to describe the emissivity profile of the accretion disk and the outer emissivity index q_{out} is either frozen to 3 (Model 1A) or

Model name	XSPEC model	q_{out}
1A	<code>tbabs×xstar×(diskbb+cutoffpl+gauss+relxill_nk)</code>	3
1B		free
2A	<code>tbabs×xstar×(diskpbb+cutoffpl+gauss+relxill_nk)</code>	3
2B		free
3A	<code>tbabs×xstar×(simplcutx×diskpbb+gauss+relxillCp_nk)</code>	3
3B		free

TABLE II. Summary of the models used to fit the data of epoch 1.

left free in the fit (Model 1B). Note that here and in what follows, for every model we fit the data first assuming the Kerr metric and setting $\alpha_{13} = 0$ and then leaving α_{13} free in the fit.

If N_{H} in `tbabs` is left free, the fit gives us the value $\approx 6 \times 10^{21} \text{ cm}^{-2}$, which is perfectly consistent with the result in Ref. [47]. So we freeze N_{H} to that value for Model 1. The best-fit values for Models 1A and 1B are reported in Tab. III. The data to best-fit model ratio of these models are shown in the top panels in Fig. 2. The top panels in Fig. 3 show the constraints on the black hole spin parameter a_* and the Johannsen deformation parameter α_{13} when α_{13} is free in the fit.

Following Refs. [42, 48], we try to improve the fit by replacing `diskbb` with `diskpbb`. In `diskpbb`, the local disk temperature $T(r)$ is proportional to r^{-p} , where p is the extra parameter of the model. The spectrum of `diskbb` is recovered for $p = 0.75$. Model 2 is thus

$$\text{tbabs} \times \text{xstar} \times (\text{diskpbb} + \text{cutoffpl} + \text{gauss} + \text{relxill_nk}),$$

and we set $p = 0.5$ as in Refs. [42, 48]. The idea is that in the hard state the corona can significantly illuminate the disk and thus alter the emissivity profile predicted by the standard thin disk model. As for Model 1, we freeze the column density in `tbabs` to $6 \cdot 10^{21} \text{ cm}^{-2}$, we assume an emissivity profile described by a broken power-law with q_{out} either frozen to 3 (Model 2A) or free (Model 2B), and for every case we first fit the data imposing the Kerr metric and then we leave α_{13} free in the fit. The best-fit values are shown in Tab. IV. In the central panels of Fig. 2, we show the data to best-fit model ratios for Model 2A and 2B. In the central panels of Fig. 3, we show the constraints on the black hole spin and deformation parameter α_{13} . We note that Model 2 improve the fit with respect to Model 1 and $\Delta\chi^2$ is around 80.

Motivated by the fact that both Model 1 and Model 2 require a high value for q_{in} and a value around 3 for q_{out} when the latter is left free, we try to improve our fit replacing `relxill_nk` with `relxillp_nk`, namely replacing a broken power-law emissivity profile with the profile expected in the lamppost geometry. However, our fits turn out to be slightly worse than those from Model 2B ($\chi^2_{\nu} = 1.075$) and we do not report the results here. We just note that the best-fit values of the model parameters are very similar to those from Model 2B, with the

exception of T_{in} , which is higher.

Last, we try to improve the fit by modeling better the Comptonized photons of the corona. We replace `cutoffpl+diskpbb` with `simplcutx×diskpbb` and `relxill_nk` with `relxillCp_nk`. `simplcutx` is a convolution model that requires as input the seed photon spectrum responsible for the Comptonization and its output includes both the Comptonized photon spectrum and the transmitted seed photon spectrum [49]. In `simplcutx`, we set the reflection fraction parameter to 1 and we link the value of the coronal temperature with its counterpart in `relxillCp_nk`. Our Model 3 is thus

$$\text{tbabs} \times \text{xstar} \times (\text{simplcutx} \times \text{diskpbb} + \text{gauss} + \text{relxillCp_nk}).$$

Unlike in Models 1 and 2, here the value of the hydrogen column density N_{H} in `tbabs` has a stronger impact on the final fit. We thus set N_{H} free in the fit. As for Models 1 and 2, we consider the two variants with $q_{\text{out}} = 3$ (3A) and free (3B), and in both cases we fit the data first assuming the Kerr metric and then relaxing this hypothesis. The best-fit values of Model 3 are reported in Tab. V, where we can see that the fit is better than Model 2 ($\chi^2_{\nu} = 1.046$). The data to best-fit model ratios are shown in Fig. 2 and the constraints on the black hole spin and the Johannsen deformation parameter are reported in the bottom panels in Fig. 3.

The discussion of the fits of epoch 1 is postponed to Section V.

IV. ANALYSIS OF EPOCH 2

To simplify the analysis, we first fit the *NuSTAR* and *Suzaku* data separately, and then we combine the two spectra for a joint fit. When we fit the spectra separately, we set N_{H} in `tbabs` to $6 \times 10^{21} \text{ cm}^{-2}$, as in Models 1 and 2 in the previous section. When we fit the *NuSTAR* and *Suzaku* data together, N_{H} has a more important influence on the final result and we do not recover $6 \times 10^{21} \text{ cm}^{-2}$ when it is allowed to vary, so we leave the parameter free in the fit. As in the previous section for the analysis of epoch 1, we consider two models for the intensity profile: broken power-law with $q_{\text{out}} = 3$ and broken power-law with q_{out} free. For every model of the intensity profile, we consider two spacetimes: Kerr metric and Johannsen

metric with α_{13} free.

We start with the analysis of the *NuSTAR* data and we use the XSPEC model

```
tbabs×xstar×(diskbb+cutoffpl+gauss+relxill_nk).
```

This is the same model as Model 1 for epoch 1, but for convenience we call it Model 4 as it fits the *NuSTAR* data of epoch 2. Following the same strategy employed in the previous section, we describe the emissivity profile with a broken power-law and the outer emissivity profile q_{out} is either frozen to 3 (Model 4A) or left free in the fit (Model 4B). For every model, we first fit the data assuming the Kerr metric ($\alpha_{13} = 0$) and then without such an assumption (α_{13} free). The best-fit values are reported in Tab. VI. The data to best-fit model ratios are shown in Fig. 4. The constraints on the black hole spin parameter a_* and the Johannsen deformation parameter α_{13} are in Fig. 5.

Since in this observation the source is in the soft state, the accretion disk is not cold, which is instead an assumption in the reflection model used. As done in Ref. [50] and then repeated in Ref. [33], we try to take the higher disk temperature into account by adding a Gaussian convolution model to the reflection spectrum at the emission point and before the relativistic convolution model. In XSPEC language, we replace `relxill_nk` with

```
relconv_nk×gsmooth×xillver.
```

However, we do not have an appreciable improvement of the fit and, on the contrary, the fit would require a negative value for q_{out} . So we do not explore further such a possibility.

We move to the analysis of the *Suzaku* data and we use the same XSPEC model:

```
tbabs×xstar×(diskbb+cutoffpl+gauss+relxill_nk).
```

Since we fit now the *Suzaku* data, we call this model Model 5, with Model 5A with $q_{\text{out}} = 3$ and Model 5B with q_{out} free. The best-fit values are reported in Tab. VII. The data to best-fit model ratios are in Fig. 6. The constraints on the black hole spin parameter a_* and the Johannsen deformation parameter α_{13} are shown in Fig. 7. We note that there is some disagreement between the XIS0 and XIS1 data. It may be related to some residual pile-up. As in the *NuSTAR* data, we try to improve the fit by replacing `relxill_nk` with `relconv_nk×gsmooth×xillver` to take into account the fact that the source is in the soft state and its accretion disk is not cold. However, as in the case of the *NuSTAR* spectrum, the fit does not improve.

Last, we fit the *NuSTAR* and *Suzaku* spectra together. N_{H} in `tbabs` is left free. Since we cannot constrain q_{out} when it is allowed to vary, we freeze it to 3. This is our Model 6, and now we do not have Models 6A and 6B. The results of our fits are shown in Tab. VIII, Fig. 8 and Fig. 9.

V. DISCUSSION AND CONCLUSIONS

Generally speaking, all our fits (either for $\alpha_{13} = 0$ or for α_{13} free) are consistent with previous studies and we find a spin parameter close to 1 and an inclination angle around 40° [48, 51–56]. While we have always modeled the emissivity profile of the disk with a broken power-law and assumed either $q_{\text{out}} = 3$ or free, the final results are quite independent of this last choice.

For the 2009 *Suzaku* observation with the source in the hard state, we have six models (1A, 1B, 2A, 2B, 3A, 3B). Model 1 provides the worse fit and we do not recover the Kerr metric at 90% confidence level (see Tab. III). Model 2 improves the fit ($\Delta\chi^2$ is around 80 without adding new free parameters) and we recover the Kerr spacetime (see Tab. IV). The spin parameter and the inclination angle of the disk do not change much between Model 1 and 2, while we can significantly reduce the iron abundance. We note, however, that in Model 2 we get quite a high value of T_{in} in `diskbb`, too high for a source in the hard state. Model 3 improves the fit of Model 2 decreasing χ^2 by about 60 and keeping the same number of free parameters. In Model 3, we recover the Kerr metric at 90% confidence level, we decrease the value of T_{in} in `diskbb`, the iron abundance increases a bit with respect to Model 2 but it is still lower than Model 1, and the estimates of the black hole spin parameter and of the inclination angle of the disk do not change much.

For the observations of the source in the soft state in 2012, we see that there is more difference between the models with $q_{\text{out}} = 3$ and those with q_{out} free. The emissivity profile of the disk is determined by the coronal geometry, which can vary with a timescales of a few days, and therefore it is not a surprise if the observations in 2009 and 2012 present some differences in the emissivity profile. Moreover, one is in the hard state and the other observation is in the soft state, so the coronal geometry could be, in principle, very different. The *NuSTAR* fits (Model 4) and the *Suzaku* fits (Model 5) are, in general, consistent, but we note that the constraints on the deformation parameter α_{13} are better in the *NuSTAR* fits, suggesting that the key-point to get stringent tests of the Kerr metric is not to have a good energy resolution near the iron line, or at least that this is not enough. We also note that, with the exception of Model 4, the estimate of the inclination angle of the disk is around 55° , which is a bit higher than what we would expect. When we combine the *NuSTAR* and *Suzaku* spectra, the estimate of the inclination angle of the disk returns to a value around 40° .

Unlike in the analysis of the *NuSTAR* observations of Cygnus X-1 presented in Ref. [33], in the present work we are able to constrain the deformation parameter α_{13} of the Johannsen metric. In the observation in the hard state, with Model 3A we find (90% CL)

$$\alpha_{13} = -0.2^{+0.3}_{-0.7}. \quad (1)$$

In the observation in the soft state, when we fit the *NuS-*

Model	1A		1B	
	$\alpha_{13} = 0$	α_{13} free	$\alpha_{13} = 0$	α_{13} free
tbabs				
$N_{\text{H}}/10^{21} \text{ cm}^{-2}$	6.0*	6.0*	6.0*	6.0*
xstar				
$N_{\text{H}}/10^{21} \text{ cm}^{-2}$	$12.5^{+1.2}_{-6}$	10^{+4}_{-4}	9^{+11}_{-5}	9^{+11}_{-5}
$\log \xi$	$3.48^{+0.4}_{-0.11}$	$3.44^{+0.23}_{-0.06}$	$3.44^{+0.6}_{-0.07}$	$3.39^{+0.29}_{-0.18}$
z	-0.017 ± 0.006	$-0.016^{+0.007}_{-0.006}$	$-0.016^{+0.007}_{-0.008}$	-0.017 ± 0.006
relxill_nk				
q_{in}	> 7.4	$8.92^{+0.22}_{-1.2}$	> 7.8	> 8.7
q_{out}	3*	3*	$3.16^{+0.24}_{-0.3}$	$3.08^{+0.03}_{-0.07}$
$R_{\text{br}} [r_{\text{g}}]$	$2.73^{+0.28}_{-0.20}$	$1.89^{+0.02}_{-0.08}$	$2.50^{+0.5}_{-0.29}$	$1.78^{+0.02}_{-0.04}$
a_*	0.976 ± 0.005	$0.988^{+0.0012}_{-0.009}$	$0.976^{+0.005}_{-0.003}$	$0.988^{+0.0012}_{-0.009}$
i [deg]	$40.0^{+1.5}_{-1.4}$	$40.0^{+0.7}_{-1.1}$	$40.1^{+2.0}_{-1.0}$	$40.3^{+0.6}_{-1.3}$
$\log \xi$	$3.13^{+0.03}_{-0.04}$	$3.136^{+0.023}_{-0.009}$	$3.12^{+0.05}_{-0.03}$	$3.150^{+0.015}_{-0.011}$
A_{Fe}	> 9.64	> 9.79	> 7.76	> 9.81
α_{13}	0*	< -0.6	0*	< -0.5
Norm	$0.0134^{+0.0008}_{-0.0011}$	$0.0132^{+0.0006}_{-0.0003}$	$0.0136^{+0.0009}_{-0.0010}$	$0.0133^{+0.0006}_{-0.0003}$
cutoffpl				
Γ	$1.557^{+0.011}_{-0.014}$	$1.555^{+0.006}_{-0.008}$	$1.556^{+0.016}_{-0.016}$	$1.548^{+0.008}_{-0.007}$
E_{cut} [keV]	286^{+42}_{-12}	284^{+16}_{-3}	287^{+37}_{-20}	278^{+4}_{-3}
Norm	0.98 ± 0.04	$0.981^{+0.013}_{-0.022}$	$0.98^{+0.03}_{-0.05}$	$0.955^{+0.04}_{-0.019}$
diskbb				
T_{in} [keV]	0.58 ± 0.03	$0.568^{+0.021}_{-0.003}$	0.58 ± 0.03	$0.554^{+0.011}_{-0.003}$
Norm	401^{+95}_{-65}	432^{+76}_{-9}	419^{+103}_{-123}	482^{+60}_{-9}
gauss				
E_{line} [keV]	6.40*	6.40*	6.40*	6.40*
σ [keV]	0.01*	0.01*	0.01*	0.01*
Norm/ 10^{-3}	0.95 ± 0.27	$0.94^{+0.25}_{-0.23}$	$0.98^{+0.27}_{-0.26}$	$0.99^{+0.24}_{-0.23}$
Cross-normalization				
C_{PIN}	$1.225^{+0.027}_{-0.028}$	$1.227^{+0.004}_{-0.006}$	$1.219^{+0.029}_{-0.025}$	$1.223^{+0.004}_{-0.008}$
C_{GSO}	1.43 ± 0.04	$1.439^{+0.015}_{-0.008}$	$1.43^{+0.04}_{-0.03}$	$1.439^{+0.015}_{-0.008}$
χ^2/ν	2373.82/2139 = 1.10978	2371.13/2138 = 1.10904	2372.82/2138 = 1.10983	2370.01/2137 = 1.10903

TABLE III. Best-fit values from Models 1A and 1B. The reported uncertainties correspond to the 90% confidence level for one relevant parameter. * means that the parameter is frozen in the fit. The ionization parameter ξ is in units erg cm s^{-1} .

TAR and *Suzaku* spectra (Model 6), we find (90% CL)

$$\alpha_{13} = 0.0^{+0.3}_{-1.5}. \quad (2)$$

These constraints are not among the best ones using `relxill_nk`. For example, limiting the discussion to tests of the Kerr metric with stellar-mass black holes, from the 2007 *Suzaku* observation of GRS 1915+105, we got [12] (90% CL)

$$\alpha_{13} = 0.00^{+0.05}_{-0.15}. \quad (3)$$

From the simultaneous analysis of reflection features and thermal spectrum of GX 339-4 with *Swift* and *NuS-TAR* data, with a broken power-law emissivity profile

we found [14] (90% CL)

$$\alpha_{13} = -0.010^{+0.024}_{-0.018}. \quad (4)$$

Cygnus X-1 thus remains quite a complicated source, especially because it is a high-mass X-ray binary and therefore the radiation emitted from the very inner region of the accretion disk is inevitably absorbed by the strong wind from the companion star. However, here we have definitively improved our analysis of Ref. [33], where it was not possible to constrain the deformation parameter α_{13} .

We remind that all uncertainties reported in this manuscript only refer to the statistical uncertainties,

Model	2A		2B	
	$\alpha_{13} = 0$	α_{13} free	$\alpha_{13} = 0$	α_{13} free
tbabs				
$N_{\text{H}}/10^{21} \text{ cm}^{-2}$	6.0*	6.0*	6.0*	6.0*
xstar				
$N_{\text{H}}/10^{21} \text{ cm}^{-2}$	10^{+9}_{-6}	10^{+9}_{-6}	12^{+9}_{-6}	12^{+9}_{-6}
$\log \xi$	$3.40^{+0.4}_{-0.24}$	$3.39^{+0.4}_{-0.24}$	$3.39^{+0.29}_{-0.18}$	$3.39^{+0.29}_{-0.18}$
z	-0.017 ± 0.006	-0.017 ± 0.006	-0.017 ± 0.006	$-0.017^{+0.006}_{-0.005}$
relxill_nk				
q_{in}	> 7.3	> 8.5	> 7.3	> 7.0
q_{out}	3*	3*	$2.86^{+0.15}_{-0.18}$	$2.86^{+0.15}_{-0.3}$
$R_{\text{br}} [r_{\text{g}}]$	$2.17^{+0.13}_{-0.3}$	$2.21^{+0.13}_{-0.25}$	$2.21^{+0.23}_{-0.21}$	$2.21^{+0.29}_{-0.7}$
a_*	$0.979^{+0.006}_{-0.008}$	> 0.960	$0.977^{+0.007}_{-0.008}$	$0.977^{+0.018}_{-0.029}$
i [deg]	$42.1^{+1.2}_{-1.5}$	$42.2^{+1.2}_{-1.6}$	$41.8^{+1.3}_{-1.6}$	$41.8^{+1.3}_{-1.6}$
$\log \xi$	$3.000^{+0.011}_{-0.023}$	$3.000^{+0.010}_{-0.021}$	$3.000^{+0.012}_{-0.024}$	$3.000^{+0.012}_{-0.024}$
A_{Fe}	$5.3^{+1.2}_{-0.5}$	$5.1^{+1.2}_{-0.3}$	$5.02^{+1.2}_{-0.21}$	$5.02^{+1.12}_{-0.22}$
α_{13}	0*	$-0.05^{+0.18}_{-0.6}$	0*	$0.0^{+0.3}_{-0.2}$
Norm	$0.0100^{+0.0008}_{-0.0009}$	$0.0098^{+0.0012}_{-0.0009}$	$0.0094^{+0.0011}_{-0.0008}$	$0.0094^{+0.0011}_{-0.0008}$
cutoffpl				
Γ	$1.542^{+0.009}_{-0.009}$	$1.541^{+0.009}_{-0.009}$	$1.546^{+0.011}_{-0.015}$	$1.546^{+0.008}_{-0.013}$
E_{cut} [keV]	260^{+16}_{-7}	259^{+17}_{-6}	262^{+14}_{-7}	262^{+14}_{-10}
Norm	$1.059^{+0.03}_{-0.022}$	$1.058^{+0.022}_{-0.023}$	$1.068^{+0.012}_{-0.029}$	$1.068^{+0.013}_{-0.03}$
diskpbb				
T_{in} [keV]	$1.29^{+0.06}_{-0.09}$	$1.29^{+0.06}_{-0.03}$	$1.32^{+0.16}_{-0.03}$	$1.32^{+0.02}_{-0.16}$
p	0.5*	0.5*	0.5*	0.5*
Norm	$7.7^{+1.2}_{-1.5}$	$7.7^{+1.3}_{-1.4}$	$6.8^{+0.6}_{-1.0}$	$6.8^{+0.7}_{-0.5}$
gauss				
E_{line} [keV]	6.40*	6.40*	6.40*	6.40*
σ [keV]	0.01*	0.01*	0.01*	0.01*
Norm/ 10^{-3}	$1.10^{+0.25}_{-0.26}$	$1.09^{+0.24}_{-0.25}$	$1.01^{+0.26}_{-0.28}$	$1.01^{+0.26}_{-0.27}$
Cross-normalization				
C_{PIN}	$1.195^{+0.017}_{-0.010}$	$1.195^{+0.016}_{-0.009}$	$1.207^{+0.015}_{-0.013}$	$1.207^{+0.016}_{-0.009}$
C_{GSO}	$1.346^{+0.026}_{-0.022}$	$1.345^{+0.026}_{-0.021}$	$1.357^{+0.024}_{-0.023}$	$1.357^{+0.024}_{-0.022}$
χ^2/ν	2294.35/2139 = 1.07263	2394.10/2138 = 1.07301	2293.08/2138 = 1.07253	2293.08/2137 = 1.07304

TABLE IV. Best-fit values from Models 2A and 2B. The reported uncertainties correspond to the 90% confidence level for one relevant parameter. * means that the parameter is frozen in the fit. The ionization parameter ξ is in units erg cm s^{-1} .

while the systematic ones are ignored. Systematic uncertainties mainly include simplifications in the theoretical model employed to analyze the data, but there are even instrumental and data analysis uncertainties; for a review, see [32] and references therein. We note that this is not only an issue for testing general relativity, but for any measurement of the properties of accreting black holes using X-ray reflection spectroscopy.

Among the systematic uncertainties related to the theoretical model, simplifications in the description of the structure of the accretion disk are often thought to be among the most important source of uncer-

tainty. Relativistic reflection models normally employ the Novikov-Thorne model for the description of the accretion disk [57, 58]. Such a model is valid for geometrically thin and optically thick accretion disks. If we employ the model to analyze sources with thick accretion disks, the final measurements can be affected by large systematic errors. If we assume general relativity and we want to measure the black hole spin, we can easily get an incorrect spin measurement [59]. In the case of tests of the Kerr metric, we can obtain a non-vanishing measurement of the deformation parameter even if the metric around the compact object is described by the Kerr so-

Model	3A		3B	
	$\alpha_{13} = 0$	α_{13} free	$\alpha_{13} = 0$	α_{13} free
tbabs				
$N_{\text{H}}/10^{21} \text{ cm}^{-2}$	$5.51^{+0.13}_{-0.14}$	$5.51^{+0.20}_{-0.14}$	$5.51^{+0.13}_{-0.15}$	$5.51^{+0.15}_{-0.21}$
xstar				
$N_{\text{H}}/10^{21} \text{ cm}^{-2}$	6.7 ± 0.5	6.9 ± 0.6	$6.8^{+0.5}_{-0.4}$	7.1 ± 0.5
$\log \xi$	3.4 ± 0.3	$3.39^{+0.3}_{-0.24}$	3.4 ± 0.3	$3.4^{+0.4}_{-0.3}$
z	$-0.017^{+0.006}_{-0.005}$	$-0.017^{+0.004}_{-0.006}$	0.017 ± 0.006	0.017 ± 0.005
relxillCp_nk				
q_{in}	> 8.1	$9.2^{+0.4}_{-3}$	> 8.3	> 6.1
q_{out}	3^*	3^*	$3.02^{+0.24}_{-0.3}$	$2.94^{+0.25}_{-0.23}$
$R_{\text{br}} [r_{\text{g}}]$	$2.51^{+0.18}_{-0.14}$	$2.4^{+0.4}_{-0.4}$	2.50 ± 0.25	$2.09^{+0.9}_{-0.15}$
a_*	$0.972^{+0.007}_{-0.009}$	$0.972^{+0.003}_{-0.009}$	$0.972^{+0.010}_{-0.012}$	$0.972^{+0.017}_{-0.024}$
i [deg]	$34.5^{+2.4}_{-1.6}$	$35.6^{+2.4}_{-4}$	35^{+4}_{-4}	35^{+3}_{-8}
$\log \xi$	$3.30^{+0.05}_{-0.09}$	$3.29^{+0.06}_{-0.08}$	$3.30^{+0.05}_{-0.09}$	$3.28^{+0.11}_{-0.08}$
A_{Fe}	$7.5^{+1.5}_{-1.1}$	$7.1^{+2}_{-0.8}$	$7.6^{+1.3}_{-1.1}$	$7.7^{+1.7}_{-1.7}$
α_{13}	0^*	$-0.2^{+0.3}_{-0.7}$	0^*	$-0.7^{+0.8}_{-0.3}$
Norm	$0.0101^{+0.0011}_{-0.0010}$	$0.0101^{+0.0011}_{-0.0010}$	$0.0102^{+0.0011}_{-0.0012}$	$0.0102^{+0.0011}_{-0.0012}$
simplcutx				
Γ	$1.621^{+0.008}_{-0.012}$	$1.621^{+0.012}_{-0.020}$	$1.621^{+0.009}_{-0.012}$	$1.621^{+0.011}_{-0.020}$
FracSctr	$0.370^{+0.05}_{-0.021}$	$0.36^{+0.04}_{-0.05}$	$0.37^{+0.05}_{-0.04}$	$0.37^{+0.04}_{-0.05}$
ReflFrac	1^*	1^*	1^*	1^*
kT_{e}	166^{+18}_{-21}	164^{+34}_{-23}	166^{+23}_{-17}	167^{+36}_{-28}
diskbb				
T_{in} [keV]	$0.86^{+0.18}_{-0.19}$	$0.86^{+0.08}_{-0.07}$	$0.86^{+0.4}_{-0.18}$	$0.86^{+0.08}_{-0.07}$
p	0.5^*	0.5^*	0.5^*	0.5^*
Norm	20^{+34}_{-6}	$17.1^{+11}_{-2.3}$	20^{+5}_{-5}	21^{+7}_{-7}
gauss				
E_{line} [keV]	6.40^*	6.40^*	6.40^*	6.40^*
σ [keV]	0.01^*	0.01^*	0.01^*	$0.07^{+0.07}_{-0.05}$
Norm/ 10^{-3}	$1.5^{+0.5}_{-0.4}$	$1.8^{+0.5}_{-0.6}$	$1.6^{+0.3}_{-0.4}$	$1.6^{+0.7}_{-0.5}$
Cross-normalization				
C_{PIN}	$1.242^{+0.021}_{-0.03}$	$1.242^{+0.021}_{-0.03}$	$1.242^{+0.022}_{-0.03}$	1.24 ± 0.03
C_{GSO}	$1.313^{+0.020}_{-0.04}$	$1.312^{+0.020}_{-0.03}$	1.31 ± 0.04	1.31 ± 0.04
χ^2/ν	$2236.08/2139$ $= 1.04538$	$2235.81/2138$ $= 1.04575$	$2235.99/2138$ $= 1.04583$	$2234.46/2137$ $= 1.04561$

TABLE V. Best-fit values from Models 3A and 3B. The reported uncertainties correspond to the 90% confidence level for one relevant parameter. * means that the parameter is frozen in the fit. The ionization parameter ξ is in units erg cm s^{-1} .

lution [60]. Assuming general relativity, numerical simulations show that the Novikov-Thorne model provides a good description of thin accretion disks when the accretion disk luminosity of the source is between a few percent and up to about 30% of its Eddington limit, and that systematic uncertainties in the estimate of the black hole spin parameter are small; see, e.g., Refs. [61–63]. However, numerical simulations with different magnetic field configurations may lead to different conclusions [64].

The take-away message of the available studies is that X-ray reflection spectroscopy measurements employing

the Novikov-Thorne model can be accurate if we select the sources and the observations with the right characteristics, while incorrect measurements can be easily obtained when we use the model for any source showing a spectrum with reflection features. We also note that a reflection model is unsuitable to test the validity of the Novikov-Thorne model, in the sense that we can obtain a good fit even if the disk is not thin because of parameter degeneracy [59, 60]. For example, even within the Kerr metric, it is difficult to test the Keplerian disk velocity of the material in the accretion disk without an

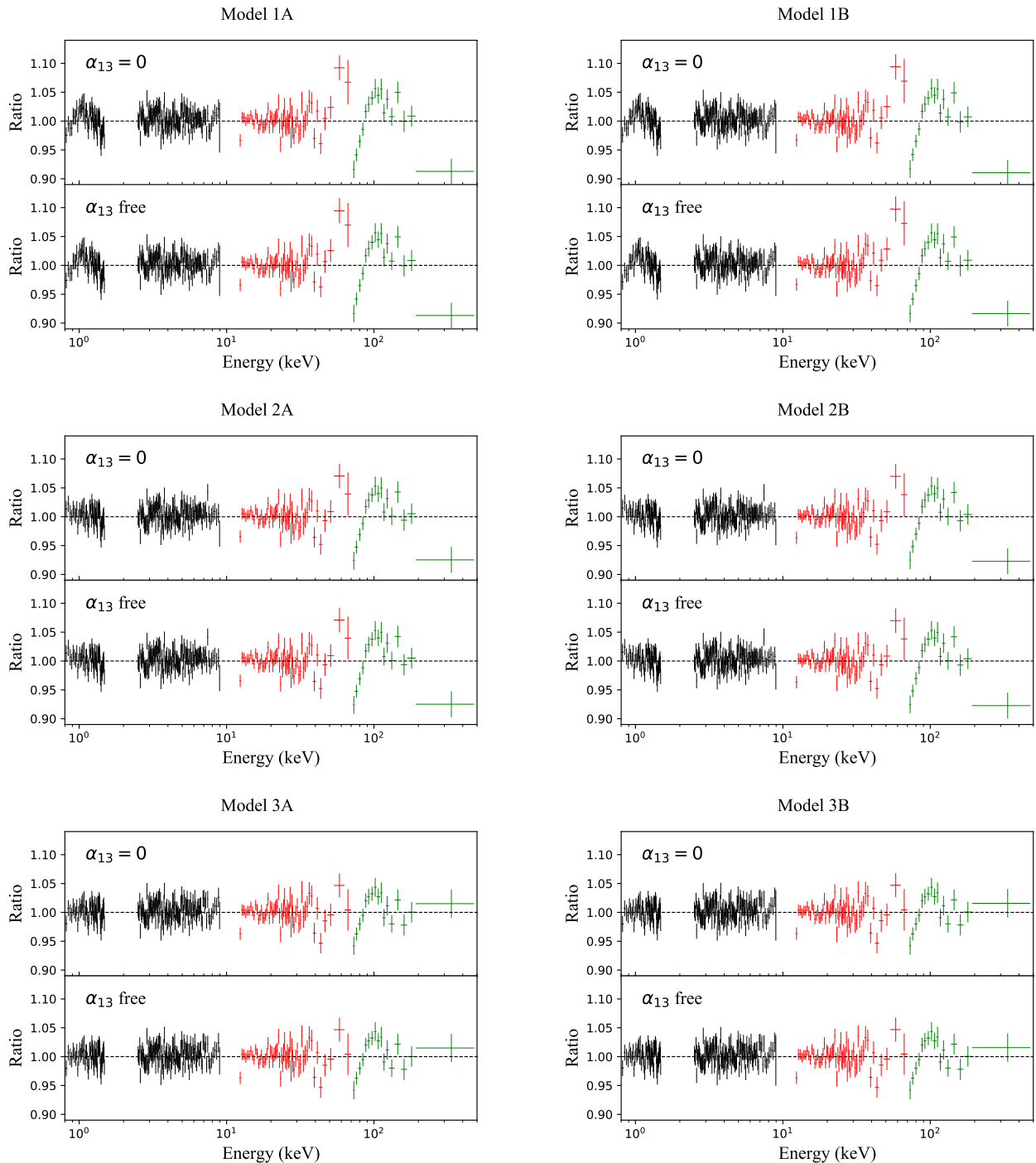


FIG. 2. Data to best-fit model ratios for Models 1A and 1B (top panels), Models 2A and 2B (central panels), and Models 3A and 3B (bottom panels). For every model, we show the results from the fit with $\alpha_{13} = 0$ and from the fit with α_{13} free.

independent measurement of the disk's inclination angle [65]. In the observations analyzed in this work, the accretion disk luminosity can be estimated to be around 1% in epoch 1 and around 10% in epoch 2. Especially in the second observation, in which the source is in the soft state, we can expect that the systematic uncertainties from the Novikov-Thorne model are modest and do

not have a significant impact on our measurements.

Acknowledgments – This work was supported by the Innovation Program of the Shanghai Municipal Education Commission, Grant No. 2019-01-07-00-07-E00035, the National Natural Science Foundation of China (NSFC), Grant No. 11973019, and Fudan Univer-

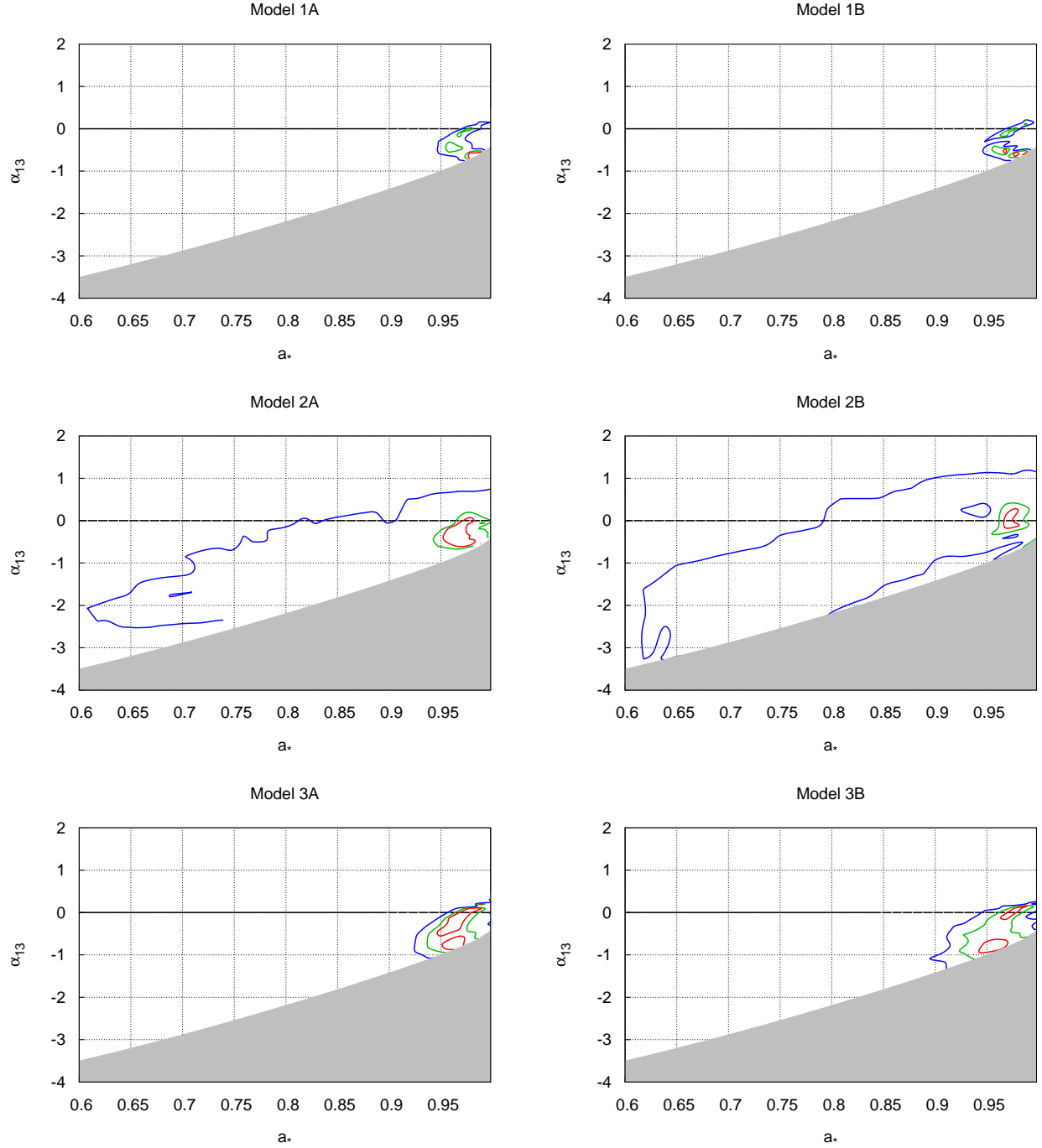


FIG. 3. Constraints on the spin parameter a_* and the Johannsen deformation parameters α_{13} for Models 1A and 1B (top panels), Models 2A and 2B (central panels), and Models 3A and 3B (bottom panels). The red, green, and blue curves are, respectively, the 68%, 90%, and 99% confidence level boundaries for two relevant parameters. The gray region is ignored in our analysis because the spacetime is not regular there.

sity, Grant No. JIH1512604.

[1] C. M. Will, Living Rev. Rel. **17**, 4 (2014) [arXiv:1403.7377 [gr-qc]].

[2] B. Jain and J. Khoury, Annals Phys. **325**, 1479-1516 (2010) [arXiv:1004.3294 [astro-ph.CO]].

Model	4A		4B	
	$\alpha_{13} = 0$	α_{13} free	$\alpha_{13} = 0$	α_{13} free
tbabs				
$N_{\text{H}}/10^{21} \text{ cm}^{-2}$	6.0*	6.0*	6.0*	6.0*
xstar				
$N_{\text{H}}/10^{21} \text{ cm}^{-2}$	$6.4^{+1.4}_{-0.6}$	$6.4^{+1.5}_{-0.6}$	$10.6^{+1.3}_{-1.5}$	$10.6^{+1.2}_{-1.3}$
$\log \xi$	$3.96^{+0.13}_{-0.4}$	$3.96^{+0.14}_{-0.4}$	$3.58^{+0.19}_{-0.07}$	$3.58^{+0.17}_{-0.08}$
z	0*	0*	0*	0*
relxill_nk				
q_{in}	3.7 ± 0.4	3.7 ± 0.4	$6.1^{+0.3}_{-0.5}$	$6.0^{+0.4}_{-0.6}$
q_{out}	3*	3*	$1.25^{+0.4}_{-0.21}$	$1.27^{+0.3}_{-0.19}$
$R_{\text{br}} [r_{\text{g}}]$	> 4.9	> 4.9	$10.0^{+1.1}_{-3}$	$9.9^{+3}_{-0.7}$
a_*	0.954 ± 0.011	$0.984^{+0.006}_{-0.04}$	$0.981^{+0.003}_{-0.007}$	$0.978^{+0.009}_{-0.014}$
i [deg]	$43.7^{+1.0}_{-1.2}$	$43.7^{+0.9}_{-1.0}$	$55.1^{+1.0}_{-1.7}$	$55.2^{+1.9}_{-1.5}$
$\log \xi$	$4.22^{+0.09}_{-0.07}$	$4.21^{+0.09}_{-0.07}$	$4.00^{+0.03}_{-0.05}$	$4.00^{+0.05}_{-0.04}$
A_{Fe}	$3.7^{+0.4}_{-0.3}$	$4.0^{+0.3}_{-0.4}$	$4.73^{+0.23}_{-0.6}$	$4.72^{+0.24}_{-0.5}$
α_{13}	0*	$0.20^{+0.15}_{-0.9}$	0*	$-0.1^{+0.3}_{-0.4}$
Norm	$0.0352^{+0.0023}_{-0.0022}$	$0.0352^{+0.0023}_{-0.0022}$	$0.044^{+0.007}_{-0.008}$	$0.044^{+0.0024}_{-0.004}$
cutoffpl				
Γ	$2.66^{+0.03}_{-0.04}$	$2.66^{+0.03}_{-0.04}$	$2.68^{+0.05}_{-0.024}$	$2.68^{+0.04}_{-0.03}$
E_{cut} [keV]	178^{+21}_{-19}	175^{+24}_{-36}	144^{+37}_{-7}	145^{+25}_{-8}
Norm	$6.3^{+0.3}_{-0.3}$	$6.3^{+0.3}_{-0.3}$	$7.10^{+0.4}_{-0.21}$	$7.11^{+0.21}_{-0.21}$
diskbb				
T_{in} [keV]	$0.511^{+0.012}_{-0.013}$	$0.511^{+0.013}_{-0.013}$	$0.493^{+0.013}_{-0.011}$	$0.493^{+0.013}_{-0.011}$
Norm	31168^{+2269}_{-2177}	31382^{+2625}_{-2268}	40250^{+1815}_{-2475}	40363^{+2590}_{-2719}
gauss				
E_{line} [keV]	6.40*	6.40*	6.40*	6.40*
σ [keV]	0.01*	0.01*	0.01*	0.01*
Norm 10^{-3}	$0.35^{+0.20}_{-0.20}$	$0.53^{+0.20}_{-0.20}$	$0.34^{+0.28}_{-0.20}$	$0.34^{+0.28}_{-0.19}$
Cross-normalization				
C_{FPMB}	$1.0023^{+0.0012}_{-0.0013}$	$1.0030^{+0.0011}_{-0.0014}$	$1.0023^{+0.0012}_{-0.0013}$	$1.0030^{+0.0012}_{-0.0013}$
χ^2/ν	2231.56/1964 = 1.13623	2231.33/1963 = 1.13670	2209.53/1963 = 1.12574	2209.09/1962 = 1.12594

TABLE VI. Best-fit values from Models 4A and 4B (*NuSTAR* data of epoch 2). The reported uncertainties correspond to the 90% confidence level for one relevant parameter. * means that the parameter is frozen in the fit. The ionization parameter ξ is in units erg cm s^{-1} .

- [3] K. Koyama, Rept. Prog. Phys. **79**, 046902 (2016) [arXiv:1504.04623 [astro-ph.CO]].
- [4] P. G. Ferreira, Ann. Rev. Astron. Astrophys. **57**, 335-374 (2019) [arXiv:1902.10503 [astro-ph.CO]].
- [5] B. P. Abbott *et al.* [LIGO Scientific and Virgo], Phys. Rev. Lett. **116**, 221101 (2016) [erratum: Phys. Rev. Lett. **121**, 129902 (2018)] [arXiv:1602.03841 [gr-qc]].
- [6] N. Yunes, K. Yagi and F. Pretorius, Phys. Rev. D **94**, 084002 (2016) [arXiv:1603.08955 [gr-qc]].
- [7] C. Bambi, Rev. Mod. Phys. **89**, 025001 (2017) [arXiv:1509.03884 [gr-qc]].
- [8] Z. Cao, S. Nampalliwar, C. Bambi, T. Dauser and J. A. Garcia, Phys. Rev. Lett. **120**, 051101 (2018) [arXiv:1709.00219 [gr-qc]].
- [9] A. Tripathi, S. Nampalliwar, A. B. Abdikamalov, D. Ayzenberg, C. Bambi, T. Dauser, J. A. Garcia and A. Marinucci, Astrophys. J. **875**, 56 (2019) [arXiv:1811.08148 [gr-qc]].
- [10] C. Bambi, K. Freese, S. Vagnozzi and L. Visinelli, Phys. Rev. D **100**, 044057 (2019) [arXiv:1904.12983 [gr-qc]].
- [11] A. Tripathi, M. Zhou, A. B. Abdikamalov, D. Ayzenberg, C. Bambi, L. Gou, V. Grinberg, H. Liu and J. F. Steiner, Astrophys. J. **897**, 84 (2020) [arXiv:2001.08391 [gr-qc]].
- [12] A. B. Abdikamalov, D. Ayzenberg, C. Bambi, T. Dauser, J. A. Garcia, S. Nampalliwar, A. Tripathi and M. Zhou, Astrophys. J. **899**, 80 (2020) [arXiv:2003.09663 [astro-ph.HE]].
- [13] D. Psaltis *et al.* [Event Horizon Telescope], Phys. Rev. Lett. **125**, 141104 (2020) [arXiv:2010.01055 [gr-qc]].
- [14] A. Tripathi, A. B. Abdikamalov, D. Ayzenberg,

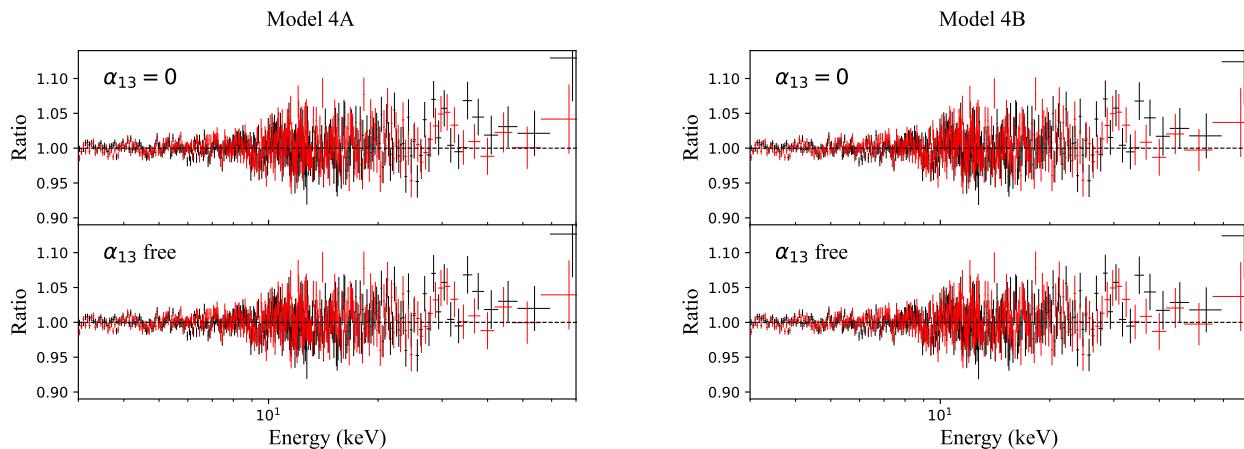


FIG. 4. Data to best-fit model ratios for Models 4A and 4B (*NuSTAR* data of epoch 2). For every model, we show the results from the fit with $\alpha_{13} = 0$ and from the fit with α_{13} free.

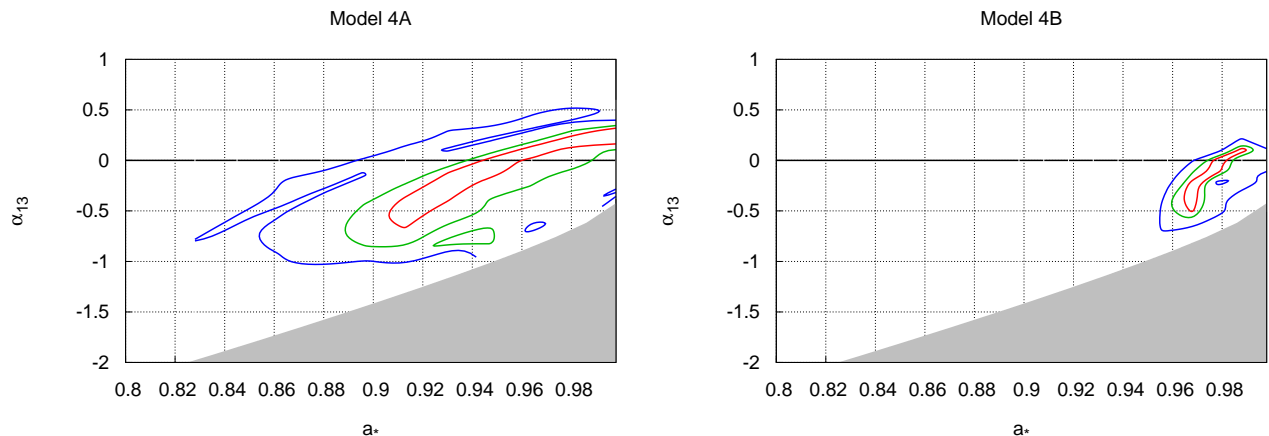


FIG. 5. Constraints on the spin parameter a_* and the Johannsen deformation parameters α_{13} for Models 4A and 4B (*NuSTAR* data of epoch 2). The red, green, and blue curves are, respectively, the 68%, 90%, and 99% confidence level boundaries for two relevant parameters. The gray region is ignored in our analysis because the spacetime is not regular there.

- C. Bambi, V. Grinberg and M. Zhou, [arXiv:2010.13474 [astro-ph.HE]].
- [15] R. Abbott *et al.* [LIGO Scientific and Virgo], [arXiv:2010.14529 [gr-qc]].
- [16] Z. Carson and K. Yagi, [arXiv:2011.02938 [gr-qc]].
- [17] R. P. Kerr, *Phys. Rev. Lett.* **11**, 237 (1963).
- [18] C. Bambi, D. Malafarina and N. Tsukamoto, *Phys. Rev. D* **89**, 127302 (2014) [arXiv:1406.2181 [gr-qc]].
- [19] C. Bambi, *Annalen Phys.* **530**, 1700430 (2018) [arXiv:1711.10256 [gr-qc]].
- [20] C. Bambi, A. D. Dolgov and A. A. Petrov, *JCAP* **0909**, 013 (2009) [arXiv:0806.3440 [astro-ph]].
- [21] G. Dvali and C. Gomez, *Fortsch. Phys.* **61**, 742-767 (2013) [arXiv:1112.3359 [hep-th]].
- [22] C. A. R. Herdeiro and E. Radu, *Phys. Rev. Lett.* **112**, 221101 (2014) [arXiv:1403.2757 [gr-qc]].
- [23] S. B. Giddings, *Phys. Rev. D* **90**, 124033 (2014) [arXiv:1406.7001 [hep-th]].
- [24] D. Ayzenberg and N. Yunes, *Phys. Rev. D* **90**, 044066 (2014) [erratum: *Phys. Rev. D* **91**, 069905 (2015)] [arXiv:1405.2133 [gr-qc]].
- [25] S. B. Giddings and D. Psaltis, *Phys. Rev. D* **97**, 084035 (2018) [arXiv:1606.07814 [astro-ph.HE]].
- [26] C. Bambi, A. Cardenas-Avendano, T. Dauser, J. A. Garcia and S. Nampalliwar, *Astrophys. J.* **842**, 76 (2017) [arXiv:1607.00596 [gr-qc]].
- [27] A. B. Abdikamalov, D. Ayzenberg, C. Bambi, T. Dauser, J. A. Garcia and S. Nampalliwar, *Astrophys. J.* **878**, 91 (2019) [arXiv:1902.09665 [gr-qc]].
- [28] T. Dauser, J. Garcia, J. Wilms, M. Bock, L. W. Brenneman, M. Falanga, K. Fukumura and C. S. Reynolds, *Mon. Not. Roy. Astron. Soc.* **430**, 1694 (2013) [arXiv:1301.4922 [astro-ph.HE]].
- [29] J. Garcia, T. Dauser, C. S. Reynolds, T. R. Kallman, J. E. McClintock, J. Wilms and W. Eikmann, *Astrophys. J.* **768**, 146 (2013) [arXiv:1303.2112 [astro-ph.HE]].
- [30] J. Garcia *et al.*, *Astrophys. J.* **782**, 76 (2014) [arXiv:1312.3231 [astro-ph.HE]].
- [31] C. S. Reynolds, *Space Sci. Rev.* **183**, 277 (2014) [arXiv:1302.3260 [astro-ph.HE]].
- [32] C. Bambi, L. W. Brenneman, T. Dauser, J. A. Garcia, V. Grinberg, A. Ingram, J. Jiang, E. Kara, H. Liu and

Model	5A		5B	
	$\alpha_{13} = 0$	α_{13} free	$\alpha_{13} = 0$	α_{13} free
tbabs				
$N_{\text{H}}/10^{21} \text{ cm}^{-2}$	6.0*	6.0*	6.0*	6.0*
xstar				
$N_{\text{H}}/10^{21} \text{ cm}^{-2}$	8.0 ± 1.9	$8.2^{+1.9}_{-1.6}$	$8.4^{+2.2}_{-1.6}$	$8.3^{+2.3}_{-1.6}$
$\log \xi$	$3.90^{+0.05}_{-0.022}$	$3.90^{+0.05}_{-0.022}$	$3.90^{+0.05}_{-0.022}$	$3.90^{+0.06}_{-0.022}$
z	0*	0*	0*	0*
relxill_nk				
q_{in}	$6.4^{+1.1}_{-0.6}$	$5.8^{+1.2}_{-0.9}$	$6.6^{+1.8}_{-1.5}$	$5.5^{+1.3}_{-0.7}$
q_{out}	3*	3*	$1.7^{+5}_{-2.6}$	$2.0^{+2.4}_{-2.5}$
$R_{\text{br}} [r_{\text{g}}]$	> 4.8	12^{+190}_{-7}	9^{+180}_{-4}	> 4.6
a_*	$0.955^{+0.005}_{-0.016}$	0.920 ± 0.015	$0.959^{+0.0023}_{-0.017}$	$0.920^{+0.03}_{-0.024}$
i [deg]	$56.6^{+2.2}_{-1.6}$	$56.4^{+1.9}_{-2.4}$	$56.9^{+4}_{-2.1}$	$56.7^{+4}_{-1.8}$
$\log \xi$	$3.30^{+0.03}_{-0.05}$	$3.30^{+0.03}_{-0.04}$	$3.30^{+0.02}_{-0.04}$	$3.30^{+0.02}_{-0.04}$
A_{Fe}	$4.8^{+1.4}_{-0.6}$	$4.8^{+1.0}_{-0.3}$	$4.8^{+1.0}_{-0.6}$	$4.9^{+0.8}_{-0.6}$
α_{13}	0*	$-0.7^{+0.8}_{-0.4}$	0*	$-0.9^{+1.3}_{-0.3}$
Norm	$0.135^{+0.019}_{-0.020}$	$0.134^{+0.021}_{-0.011}$	$0.135^{+0.005}_{-0.020}$	$0.133^{+0.006}_{-0.016}$
cutoffpl				
Γ	$2.80^{+0.02}_{-0.014}$	$2.80^{+0.02}_{-0.014}$	$2.80^{+0.02}_{-0.014}$	$2.80^{+0.02}_{-0.014}$
E_{cut} [keV]	246^{+84}_{-85}	234^{+110}_{-36}	240^{+81}_{-39}	241^{+86}_{-46}
Norm	$13.3^{+0.7}_{-1.1}$	$13.2^{+0.7}_{-0.8}$	$13.2^{+0.8}_{-1.4}$	$13.3^{+0.6}_{-1.1}$
diskbb				
T_{in} [keV]	0.552 ± 0.013	0.552 ± 0.013	0.552 ± 0.013	0.552 ± 0.013
Norm	25395^{+662}_{-671}	25432^{+594}_{-1209}	25299^{+851}_{-1867}	25345^{+1723}_{-1363}
gauss				
E_{line} [keV]	6.40*	6.40*	6.40*	6.40*
σ [keV]	0.01*	0.01*	0.01*	0.01*
Norm 10^{-3}	1.5 ± 0.6	1.3 ± 0.6	1.3 ± 0.6	1.3 ± 0.6
Cross-normalization				
C_{XIS1}	$0.9134^{+0.0024}_{-0.0021}$	$0.9134^{+0.0024}_{-0.0021}$	$0.9134^{+0.0024}_{-0.0021}$	$0.9134^{+0.0024}_{-0.0021}$
C_{PIN}	$0.933^{+0.03}_{-0.015}$	$0.933^{+0.024}_{-0.011}$	$0.933^{+0.024}_{-0.04}$	$0.936^{+0.025}_{-0.04}$
C_{GSO}	0.96 ± 0.04	0.96 ± 0.04	0.97 ± 0.04	0.97 ± 0.04
χ^2/ν	$3419.69/3085$ = 1.10849	$3418.86/3084$ = 1.10858	$3419.18/3084$ = 1.10868	$3418.56/3083$ = 1.10884

TABLE VII. Best-fit values from Models 5A and 5B (*Suzaku* data of epoch 2). The reported uncertainties correspond to the 90% confidence level for one relevant parameter. * means that the parameter is frozen in the fit. The ionization parameter ξ is in units erg cm s^{-1} .

- A. M. Lohfink, *et al.* [arXiv:2011.04792 [astro-ph.HE]].
- [33] H. Liu, A. B. Abdikamalov, D. Ayzenberg, C. Bambi, T. Dauser, J. A. Garcia and S. Nampalliwar, Phys. Rev. D **99**, 123007 (2019) [arXiv:1904.08027 [gr-qc]].
- [34] Y. Zhang, A. B. Abdikamalov, D. Ayzenberg, C. Bambi, T. Dauser, J. A. Garcia and S. Nampalliwar, Astrophys. J. **875**, 41 (2019) [arXiv:1901.06117 [gr-qc]].
- [35] J. Wang, A. B. Abdikamalov, D. Ayzenberg, C. Bambi, T. Dauser, J. A. Garcia, S. Nampalliwar and J. F. Steiner, JCAP **05**, 026 (2020) [arXiv:1806.00126 [gr-qc]].
- [36] A. Tripathi, J. Yan, Y. Yang, Y. Yan, M. Garnham, Y. Yao, S. Li, Z. Ding, A. B. Abdikamalov and D. Ayzenberg, *et al.* Astrophys. J. **874**, 135 (2019) [arXiv:1901.03064 [gr-qc]].
- [37] Y. Zhang, A. B. Abdikamalov, D. Ayzenberg, C. Bambi and S. Nampalliwar, Astrophys. J. **884**, 147 (2019) [arXiv:1907.03084 [gr-qc]].
- [38] J. A. Orosz, J. E. McClintock, J. P. Aufdenberg, R. A. Remillard, M. J. Reid, R. Narayan and L. Gou, Astrophys. J. **742**, 84 (2011) [arXiv:1106.3689 [astro-ph.HE]].
- [39] M. J. Reid, J. E. McClintock, R. Narayan, L. Gou, R. A. Remillard and J. A. Orosz, Astrophys. J. **742**, 83 (2011) [arXiv:1106.3688 [astro-ph.HE]].
- [40] K. Mitsuda, M. Bautz, H. Inoue, R. L. Kelley,

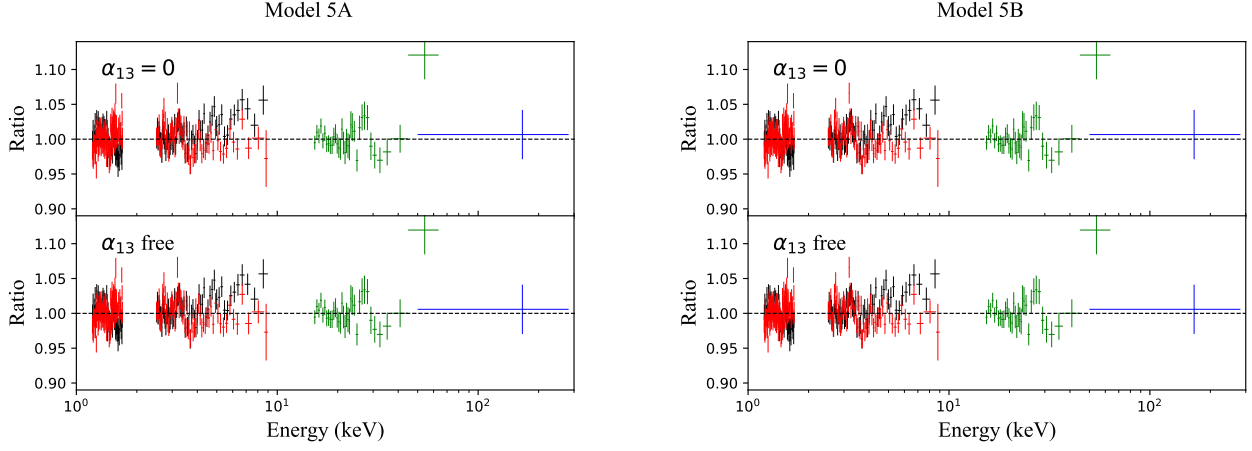


FIG. 6. Data to best-fit model ratios for Models 5A and 5B (*Suzaku* data of epoch 2). For every model, we show the results from the fit with $\alpha_{13} = 0$ and from the fit with α_{13} free.

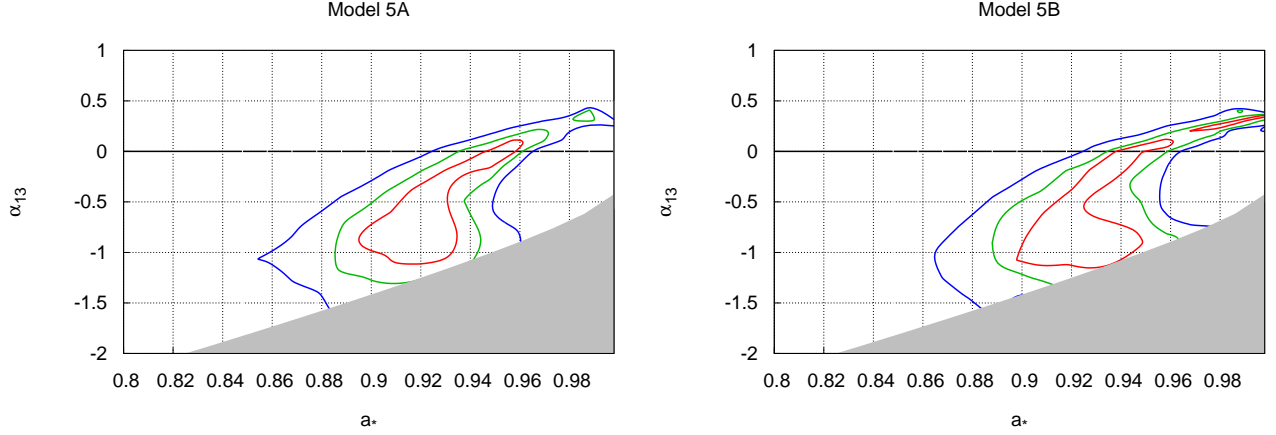


FIG. 7. Constraints on the spin parameter a_* and the Johannsen deformation parameters α_{13} for Models 5A and 5B (*Suzaku* data of epoch 2). The red, green, and blue curves are, respectively, the 68%, 90%, and 99% confidence level boundaries for two relevant parameters. The gray region is ignored in our analysis because the spacetime is not regular there.

- K. Koyama, H. Kunieda, K. Makshima, Y. Ogawara, R. Petre and T. Takahashi, *et al.* *Publ. Astron. Soc. Jap.* **59**, S1-S7 (2007).
- [41] F. A. Harrison *et al.*, *Astrophys. J.* **770**, 103 (2013) [arXiv:1301.7307 [astro-ph.IM]].
- [42] J. M. Miller, G. G. Pooley, A. C. Fabian, M. A. Nowak, R. C. Reis, E. M. Cackett, K. Pottschmidt and J. Wilms, *Astrophys. J.* **757**, 11 (2012) [arXiv:1207.3752 [astro-ph.HE]].
- [43] K. A. Arnaud, *Astronomical Data Analysis Software and Systems V*, **101**, 17 (1996).
- [44] J. Wilms, A. Allen and R. McCray, *Astrophys. J.* **542**, 914 (2000) [astro-ph/0008425].
- [45] T. Johannsen, *Phys. Rev. D* **88**, 044002 (2013) [arXiv:1501.02809 [gr-qc]].
- [46] K. Mitsuda *et al.*, *Publ. Astron. Soc. Jap.* **36**, 741 (1984).
- [47] N. S. Schulz, C. R. Canizares, D. P. Huenemoerder and K. J. Tibbetts, *Astrophys. J.* **595**, 365-383 (2003) [arXiv:astro-ph/0306008 [astro-ph]].
- [48] A. C. Fabian *et al.*, *Mon. Not. Roy. Astron. Soc.* **424**, 217 (2012) [arXiv:1204.5854 [astro-ph.HE]].
- [49] J. F. Steiner, J. A. Garcia, W. Eikmann, J. E. McClintock, L. W. Brenneman, T. Dauser and A. C. Fabian, *Astrophys. J.* **836**, 119 (2017) [arXiv:1701.03777 [astro-ph.HE]].
- [50] D. J. Walton *et al.*, *Astrophys. J.* **826**, 87 (2016) [arXiv:1605.03966 [astro-ph.HE]].
- [51] R. Duro *et al.*, *Astron. Astrophys.* **533**, L3 (2011) [arXiv:1108.1157 [astro-ph.HE]].
- [52] J. A. Tomsick *et al.*, *Astrophys. J.* **780**, 78 (2014) [arXiv:1310.3830 [astro-ph.HE]].
- [53] M. L. Parker *et al.*, *Astrophys. J.* **808**, 9 (2015) [arXiv:1506.00007 [astro-ph.HE]].
- [54] J. A. Tomsick *et al.*, *Astrophys. J.* **855**, 3 (2018) [arXiv:1801.07267 [astro-ph.HE]].
- [55] L. Gou *et al.*, *Astrophys. J.* **742**, 85 (2011) [arXiv:1106.3690 [astro-ph.HE]].
- [56] L. Gou *et al.*, *Astrophys. J.* **790**, 29 (2014) [arXiv:1308.4760 [astro-ph.HE]].
- [57] I. D. Novikov and K. S. Thorne, *Astrophysics and black holes*, in *Black Holes*, edited by C. De Witt and B. De Witt (Gordon and Breach, New York, New York,

Model	$\alpha_{13} = 0$	α_{13} free
tbabs		
$N_{\text{H}}/10^{21} \text{ cm}^{-2}$	$5.0^{+0.1}_{-0.1}$	$5.0^{+0.1}_{-0.1}$
xstar		
$N_{\text{H}}/10^{21} \text{ cm}^{-2}$	6.9 ± 0.8	6.9 ± 0.8
$\log \xi$	$3.91^{+0.06}_{-0.03}$	$3.91^{+0.06}_{-0.03}$
z	0^*	0^*
relxill_nk		
q_{in}	$3.51^{+0.4}_{-0.12}$	$3.5^{+0.3}_{-0.3}$
q_{out}	3^*	3^*
$R_{\text{br}} [r_{\text{g}}]$	> 7.54	> 8.20
a_*	$0.935^{+0.012}_{-0.019}$	$0.935^{+0.019}_{-0.05}$
i [deg]	$42.3^{+0.7}_{-0.7}$	$42.3^{+0.8}_{-0.6}$
$\log \xi$	$4.30^{+0.03}_{-0.06}$	$4.30^{+0.024}_{-0.05}$
A_{Fe}	$7.2^{+0.7}_{-0.5}$	$7.2^{+0.7}_{-0.4}$
α_{13}	0^*	$0.0^{+0.3}_{-1.5}$
Norm	$0.0233^{+0.0012}_{-0.0013}$	$0.0233^{+0.0012}_{-0.0013}$
cutoffpl		
Γ	$2.55^{+0.014}_{-0.03}$	$2.54^{+0.014}_{-0.03}$
E_{cut} [keV]	93^{+3}_{-4}	$92.7^{+3}_{-1.3}$
Norm	$5.38^{+0.16}_{-0.24}$	$5.38^{+0.15}_{-0.12}$
diskbb		
T_{in} [keV]	$0.532^{+0.014}_{-0.012}$	$0.532^{+0.014}_{-0.012}$
Norm	25818^{+841}_{-680}	25818^{+884}_{-354}
gauss		
E_{line} [keV]	6.40^*	6.40^*
σ [keV]	0.01^*	0.01^*
Norm 10^{-3}	$0.52^{+0.19}_{-0.15}$	$0.52^{+0.19}_{-0.15}$
Cross-normalization		
C_{FPMB}	$1.0034^{+0.0012}_{-0.0013}$	$1.0034^{+0.0012}_{-0.0013}$
C_{XIS0}	1.258 ± 0.003	1.258 ± 0.003
C_{XIS1}	$1.148^{+0.024}_{-0.011}$	$1.148^{+0.024}_{-0.011}$
C_{PIN}	1.425 ± 0.006	$1.425^{+0.007}_{-0.006}$
C_{GSO}	1.54 ± 0.13	1.54 ± 0.13
χ^2/ν	$5961.42/5024$ $= 1.18659$	$5961.42/5024$ $= 1.18682$

TABLE VIII. Best-fit values from Model 6 (*NuSTAR*+*Suzaku* data of epoch 2) The reported uncertainties correspond to the 90% confidence level for one relevant parameter. * means that the parameter is frozen in the fit. The ionization parameter ξ is in units erg cm s^{-1} .

- 1973).
- [58] D. N. Page and K. S. Thorne, *Astrophys. J.* **191**, 499-506 (1974).
- [59] S. Riaz, D. Ayzenberg, C. Bambi and S. Nampalliwar, *Astrophys. J.* **895**, 61 (2020) [arXiv:1911.06605 [astro-ph.HE]].
- [60] S. Riaz, D. Ayzenberg, C. Bambi and S. Nampalliwar, *Mon. Not. Roy. Astron. Soc.* **491**, 417-426 (2020) [arXiv:1908.04969 [astro-ph.HE]].
- [61] C. S. Reynolds and A. C. Fabian, *Astrophys. J.* **675**, 1048 (2008) [arXiv:0711.4158 [astro-ph]].
- [62] R. F. Penna, J. C. McKinney, R. Narayan, A. Tchekhovskoy, R. Shafee and J. E. McClintock, *Mon. Not. Roy. Astron. Soc.* **408**, 752 (2010) [arXiv:1003.0966 [astro-ph.HE]].
- [63] A. K. Kulkarni, R. F. Penna, R. V. Shcherbakov, J. F. Steiner, R. Narayan, A. Sadowski, Y. Zhu, J. E. McClintock, S. W. Davis and J. C. McKinney, *Mon. Not. Roy. Astron. Soc.* **414**, 1183 (2011) [arXiv:1102.0010 [astro-ph.HE]].
- [64] S. C. Noble, J. H. Krolik and J. F. Hawley, *Astrophys. J.* **711**, 959-973 (2010) [arXiv:1001.4809 [astro-ph.HE]].

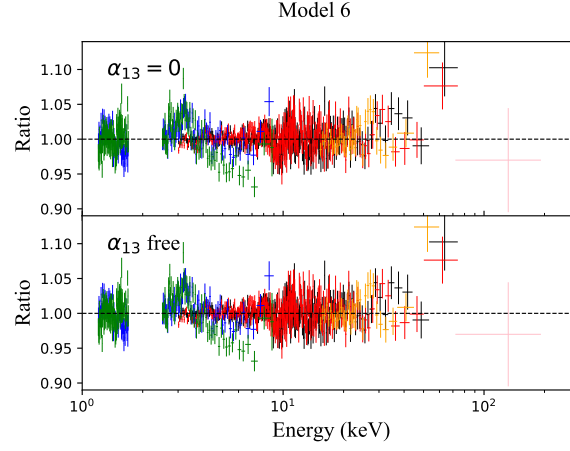


FIG. 8. Data to best-fit model ratios for Model 6 (*NuSTAR*+*Suzaku* data of epoch 2). The emissivity profile is modeled with broken power-law with $q_{\text{out}} = 3$.

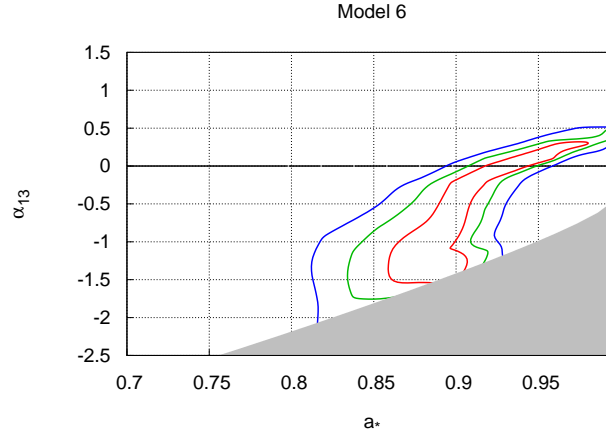


FIG. 9. Constraints on the spin parameter a_* and the Johannsen deformation parameters α_{13} for Model 6 (*NuSTAR*+*Suzaku* data of epoch 2). The emissivity profile is modeled with a broken power-law with outer emissivity index frozen to 3. The red, green, and blue curves are, respectively, the 68%, 90%, and 99% confidence level boundaries for two relevant parameters.

[65] A. Tripathi, B. Zhou, A. B. Abdikamalov, D. Ayzenberg,

C. Bambi and S. Nampalliwar, *Phys. Rev. D* **102**, 103009 (2020) [arXiv:2008.01934 [astro-ph.HE]].